Pilot-assisted PAPR reduction in PAM-DMT based visible light communication systems

Alrakah, Hussien ; Sinanovic, Sinan; Popoola, Waisu O.

Published in:
Proceedings of IEEE LATICOM 2021

Publication date:
2021

Document Version
Author accepted manuscript

Pilot-Assisted PAPR Reduction in PAM-DMT based Visible Light Communication Systems

Hussien Alrakah*†, Sinan Sinanovic‡, Wasiu O. Popoola *
*Institute for Digital Communications, School of Engineering.
The University of Edinburgh, Edinburgh, EH9 3FD, UK.
†Faculty of Computer Science and Information Technology.
Jazan University, Jazan, Kingdom of Saudi Arabia.
‡School of Engineering and Built Environment.
Glasgow Caledonian University, Glasgow, Scotland, UK.
h.alrakah@ed.ac.uk, sinan.sinanovic@gcu.ac.uk, w.popoola@ed.ac.uk

***Abstract*—Pulse-amplitude-modulated discrete multitone modulation (PAM-DMT) offers an energy-efficient modulation solution for optical wireless communication systems. However, similar to other multicarrier modulation (MCM) techniques, PAM-DMT suffers from a high peak-to-average power ratio (PAPR). This paper experimentally demonstrates the efficacy of pilot-assisted (PA) PAPR reduction system in PAM-DMT based visible light communication (VLC) systems. PA PAM-DMT is compared in this manuscript to PAM-DMT based on Bit Error Rate (BER), Signal-to-Noise Ratio (SNR) and PAPR. A gain of 2.75 dB is achieved using 10 pilot iterations for 8-PAM. The BER performance of the PA PAM-DMT is better than that of the conventional PAM-DMT with a reduced PAPR. The proposed system allows for higher input signal swing levels while minimising the non-linearity effects that result from operating beyond Light Emitting Diode's (LED's) dynamic range.**

***Index Terms*—PAM-DMT, optical OFDM, optical wireless communication, visible light communication, peak-to-average power ratio PAPR, pilot-assisted PA.**

I. Introduction

Optical wireless communication (OWC) continues to attract interests with the exponential growth of smart devices and increasing demands for high data rate transmission. Visible light communication (VLC) technology offers an unregulated and large spectrum which can meet these increasing demands. Furthermore, significant energy and cost savings can be enabled by VLC technology due to the reuse of the existing lighting infrastructure [1]. VLC uses off-the-shelf front end devices i.e. light emitting diodes (LEDs) and photodiodes (PDs). The data transmission mechanism in VLC is based on Intensity Modulation with Direct Detection (IM/DD) which restricts the modulating electrical signal to be real and positive [2].

Multicarrier modulation techniques are attractive candidates for OWC due to their resilience to multiple path propagation, intersymbol interference (ISI) mitigation and simplified equalization process using single-tap equalizers [1], [3].

Discrete multitone is a baseband variant of the OFDM technique that is widely known for its use in Asymmetric Digital Subscriber Line (ADSL) systems. Different DMT versions have been proposed for optical systems such as optical wireless and single-mode and multi-mode fibres [4]. Several modulation techniques were proposed in order to enable OFDM modulation for IM/DD systems.

In DCO-OFDM, the bipolar DMT is converted to unipolar by adding a direct current (DC) bias [4], [5]. Another option is by using Fourier transformation properties in Asymmetric Clipped Optical OFDM (ACO-OFDM) by loading symbols on the odd-indexed subcarriers. This results in an asymmetric property in the time domain and allows the signal to be clipped at zero level without any additional distortion to the information symbols as shown in [5]. DCO-OFDM is energy inefficient because of the power of the added DC-bias [6]. ACO-OFDM was shown to outperform DCO-OFDM for low spectral efficiency values [6]. In ACO-OFDM the asymmetric clipping noise falls onto the non-data carrying even-numbered subcarriers. This solution comes at the cost of reducing the spectral efficiency of the system by half [7].

Pulse-amplitude-modulated DMT (PAM-DMT) was proposed in [4] to improve the spectral and energy inefficiency of ACO-OFDM and DCO-OFDM respectively. In PAM-DMT, the PAM symbols are modulated onto the imaginary components while, the real parts are set to zeros. PAM-DMT activates all subcarriers and allows for asymmetrical clipping at zero level and transmit only the positive samples of the DMT signal.

Despite the individual advantages of the aforementioned techniques, they are all affected by high peak-to-average power ratio (PAPR) due to coherent addition of the individual subcarriers. PAPR induces signal distortion which is undesirable in OWC systems due to the limited dynamic range of the system front-end devices. This in turn restricts the average transmitted optical power and causes system performance degradation [3].

Various solutions have been proposed to address the PAPR challenge including lower and upper level clipping, coding, multiple signal representation (MSR) and selective mapping (SLM) techniques, as detailed in [3], [8], [9] and [10]. Pilot-assisted (PA) scheme is an interesting solution for the reduction of the PAPR in OFDM systems [3]. This technique uses a random pilot to rotate the phase of the data frame in order to avoid the coherent addition of the subcarriers.

978-1-6654-4035-6/21/$31.00 ©2021 IEEE

In this paper, The PAPR of PAM-DMT systems is investigated and studied experimentally in a VLC system. The PA PAPR reduction technique proposed in [3] is implemented to reduce the high peaks in a PAM-DMT visible light communication system. The PAPR values of PAM-DMT and Pilot-assisted PAM-DMT (PA PAM-DMT) are evaluated and compared.

The rest of this paper is organized as follows: In Section II optical PAM-DMT system is described, while the proposed pilot-assisted technique is introduced in Section III. Experimental setup is presented in Section IV, while the results are discussed in Section V. The paper is concluded in Section VI.

II. Optical PAM-DMT System Discretion

In PAM-DMT, the imaginary components of the complex-valued PAM symbols are modulated and, the real parts are not used and set to zeros. This results in $X[k] = \jmath B_{\text{PAM}}[k]$, where $B_{\text{PAM}}[k]$ is the M-PAM symbols carrying useful data that are loaded on the imaginary components where $(k = 1, 2, \ldots, N/2-1)$ and $N = 2(N_{\text{subs}}+1)$ where N_{subs} is the active subcarriers carrying information [4].

An optical source in a VLC system is modulated by a real-valued baseband waveform which means that the time domain signal of PAM-DMT must be real and positive. The real-valued time domain signal is achieved by imposing a Hermitian symmetry on the PAM mapped symbols in the frequency domain which is given by: $X[k] = X^*[N/2-k]$, where X^* indicates the conjugate of X and $X[0] = X[N/2] = 0$.

The PAM-DMT frame in the frequency domain with a Hermitian symmetry is given as follows:

$$X_{\text{H}} = \left[0, X_1, \ldots, X_{N/2-1}, 0, X^*_{N/2-1}, \ldots, X^*_1\right] \quad (1)$$

To sufficiently capture all the signal peaks across the Inverse Fast Fourier Transform (IFFT) length, zero padding is inserted into the frequency domain. The value for the oversampling factor is chosen at $L = 4$ similar to [3], hence (1) can be given as follows:

$$X_{\text{H}} = \left[0, X(k), \underbrace{0, 0, \ldots, 0}_{\text{N(L-1)/2}}, 0, \underbrace{0, 0, \ldots, 0}_{\text{N(L-1)/2}}, X^*(N_{\text{IFFT}}-k)\right] \quad (2)$$

The corresponding time domain signal $x[n]$ is obtained by applying IFFT of size $(N\text{x}L)$ to the frequency domain waveform which is given as follows [4]:

$$x[n] = \frac{-2}{\sqrt{N_{\text{IFFT}}}} \sum_{k=1}^{N_{\text{IFFT}}/2-1} B_{\text{PAM}}[k] \sin\left(2\pi k \frac{n}{N_{\text{IFFT}}}\right) \quad (3)$$

where $n = 0, 1, 2, \ldots, N_{\text{IFFT}} - 1$. Cyclic prefix (CP) is then inserted at the beginning of each PAM-DMT frame to eliminate the ISI in dispersive channel [3]. The time domain waveform follows an antisymmetry property which can be visualized in Fig. 1. As a result of the antisymmetry $x[n] = -x[N-n]$, the clipping of the negative peaks in the time domain PAM-DMT signal $x[n]$ does not affect the useful information as the same information are loaded on the positive components of the second half of the waveform. This means that zero level clipping distortion only affects the real components of the subcarriers, and the useful data can be recovered from the imaginary components [4].

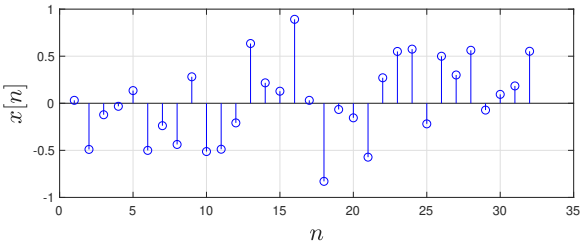

(a) PAM-DMT time domain waveform.

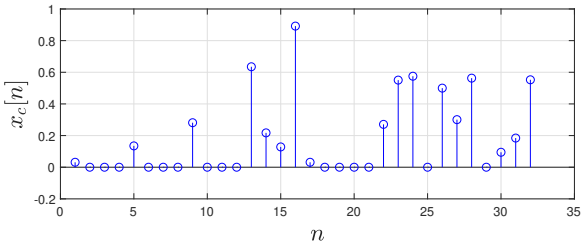

(b) PAM-DMT clipped time domain waveform.

Fig. 1. PAM-DMT time domain signal and clipped part.

A continuous time domain signal $x(t)$ of the system is obtained by feeding the discrete signal $x[n]$ in (3) into a digital to analogue converter (DAC) which is then used to modulate the intensity of the light source [3].

At the receiver, the real components of the subcarriers are ignored while the imaginary part is used and re-scaled by a factor of 2 before it is equalized and demodulated to recover the useful information [11].

III. High PAPR Reduction with Pilot Assisted Technique

PAM-DMT allows asymmetric clipping at zero values and convey the useful information on the positive parts of the DMT signal $x[n]$ which makes full use of the spectral efficiency of the system [4]. However, the inherent high PAPR problem of the system must be addressed to benefit from the full dynamic range of the light source. The high PAPR problem will cause the following: 1) the optical source will have to operate outside its linear dynamic region to contain full amplitude swings of the signal, 2) the upper level clipping by the frond-end devices of the system results in clipping noise and distortion introduced to the transmitted signal [12].

To address the PAPR problem, the pilot assisted (PA) will be used to reduce the high PAPR of the PAM-DMT system. PA was introduced in [3] to rotate the phase of the OFDM signal. However, its extension to PAM-DMT modulation technique is not straightforward. In this section, PA technique implemen-

tation for PAM-DMT system is described and realized in a VLC experiment.

The electrical peak-to-average power ratio PAPR of the oversampled time domain PAM-DMT symbol is defined as follows [3]:

$$\text{PAPR} = \frac{\max\limits_{0 \le n \le N_{\text{IFFT}}-1}(|x[n]|^2)}{E[|x[n]|^2]} \tag{4}$$

where E[·] is the statistical expectation. The PAPR is evaluated using the complementary cumulative distribution function diagram (CCDF) and it is the most used measure for PAPR reduction [3]. The CCDF is defined as the probability that the PAM-DMT frame PAPR exceeds a predefined reference value. High PAPR peaks appear when individual subcarriers added up coherently in time domain [13].

The procedure of using PA for PAPR reduction in PAM-DMT is described as follows [12]:

- Generate R different iterations of pilot candidates X_p^r, where $r = 1, 2, \ldots, R$.
- X_p^r sequence amplitude is set to ± 1 only.
- The sequence phase $\theta_p(k)$ is randomly generated and could only take either 0 or π values, $k = 1, 2, \ldots, N_{\text{subs}}$.
- Calculate PAPR_r value of each pilot iteration of X_p^r.
- Select the pilot sequence $X_p = X_p^{\tilde{r}}$ that gives the minimum PAPR of all iterations R for the transmission; where [12],

$$\tilde{r} = \arg\min_{1 \le r \le R} (\text{PAPR}_r) \tag{5}$$

In this work, number of PAM-DMT frames are grouped together to form a block U, and $U = 5$ frames per block, each frame has N_{IFFT} size. One pilot sequence is embedded into PAM-DMT U block to reduce its PAPR, as a result the number of frame per block will be $\hat{U} = U + 1$ for PA PAM-DMT, details shown in [12].

CP is often not used when evaluating the PAPR of the system as it has negligible effect on the Signal-to-Noise Ratio (SNR) and PAPR. At the receiver, the PA sequence is estimated using a maximum likelihood (ML) technique as detailed in [3]. The recovered PA phase will be used to recover the phase of the received data prior to the equalization process.

IV. Experimental Setup

An experiment is employed to evaluate the performance of PA PAM-DMT in a VLC system as illustrated in Fig. 2. The system transmitter consists of a computer that controls a waveform generator, LED (Vishay VLMB1500-GS08) and a Bias-Tee. An amplified photodetector (PDA10A-EC-Si, 200-1100 nm, 150 MHz BW) is used as the optical signal receiver.

The system performance in this work is investigated at $d = 100$ cm link distance. A longer distance measurement is possible using a higher power LED. A PA PAM-DMT signal is generated in MATLAB and converted into an analogue waveform using arbitrary waveform generator (AWG) (Keysight 33622A) employed at 100 MHz. The generated signal is DC biased using a bias-tee (ZFBT-4R2GW+). The DC bias is

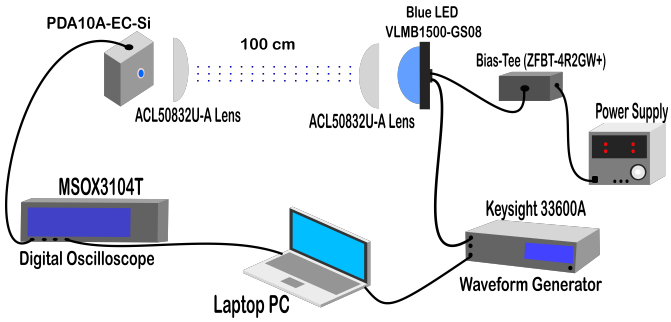

Fig. 2. Laboratory setup of PA PAM-DMT technique for visible light communication system.

required for optical OFDM modulation techniques such as DCO-OFDM to convert the bipolar signal into a unipolar. This bias is not required for the unipolar PA PAM-DMT. However, a minimum DC bias is still required due to the turn on voltage of the used LED.

Two identical aspheric condenser lenses (ACL50832U-A) are used at the transmitter (light source) and the photo-receiver ends to collimate the output light of the LED and focus the light into the detection area of the PD respectively. The receiver is an amplified fixed gain detector which includes a reverse-biased PIN photodiode, mated to a transimpedance amplifier (TIA). PD converts the received optical radiation into an electrical current signal which is converted afterwards into a voltage signal by the transimpedance amplifier TIA [3]. The received signal is then captured with a digital oscilloscope (Keysight MSOX3104T - 1 GHz) and processed afterwards off-line using MATLAB. The received signal is equalized subsequently using zero forcing equalizer then demodulated. The entire system 3 dB bandwidth is measured at 11.7 MHz.

The system is investigated at different input current to find the mid point of the linear region of the LED as shown in Fig. 3. The input current points are chosen in the linear region of the LED to avoid upper levels clipping as indicated in Fig. 3. The operating point in this experiment is chosen to be around 3.31V and it corresponds to a 20 mA input current to the LED as the input signal is clipped at zero level and only minimum DC bias is required due to the turn on voltage of the light source.

The system SNR is calculated at different input signal peak-to-peak voltage (V_{pp}) using the channel impulse response (CIR) at the corresponding (V_{pp}) in frequency domain at the receiver side using (6).

$$SNR[k] = \frac{|H[k]|^2 \times |X[k]|^2}{|W[k]|^2} \tag{6}$$

where $H[k]$ is the channel impulse response at sample k, $X[k]$ is the transmitted signal at sample k and $W[k]$ is the frequency domain estimated noise for sample k at the receiver. $H[k]$ is estimated using the prior knowledge of an embedded pilot to the transmitted signal as follows in (7):

$$\tilde{H}[k] = \frac{Y[k]}{X[k]} \tag{7}$$

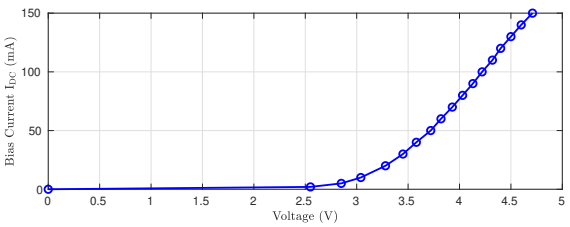

(a) LED IV Curve.

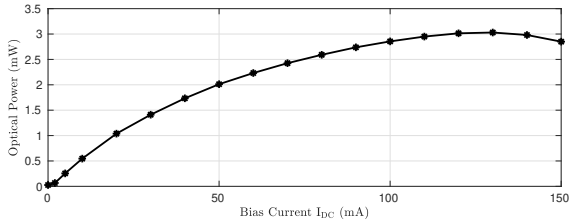

(b) Received optical power vs input voltage curve.

Fig. 3. Current-Voltage characteristics of the LED.

where $Y[k]$ is given as follows in (8):

$$Y[k] = X[k] \times H[k] + W[k] \tag{8}$$

The noise estimate of the system is evaluated as shown below:

$$\tilde{W}[k] = Y[k] - \tilde{H}[k]X[k] \tag{9}$$

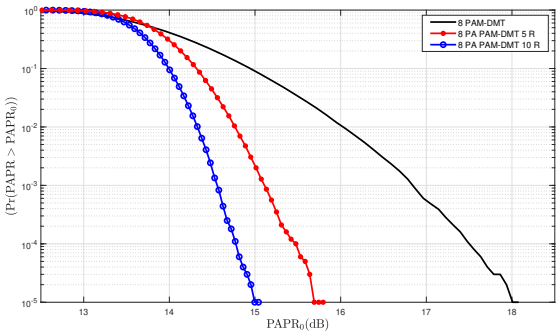

Fig. 4. PAPR CCDF plot for PAM-DMT and PA PAM-DMT using 8-PAM, $U = 5$ data frames per block, N_{subs} = 127 active subcarriers, $L = 4$ and IFFT length N_{IFFT} of 1024.

V. Results and Discussion

In this work, the conventional PAM-DMT and PA PAM-DMT systems are compared in terms of PAPR values using the same random data streams and parameters. The CCDF value of 10^{-4} is used in this work as a metric to compare the PAPR of both techniques. It can be observed from Fig. 4 that a PAPR reduction gain of 2.75 dB is achieved by applying pilot assisted scheme to PAM-DMT. At least one out of every 10^4 PAM-DMT frames has its PAPR greater than 17.5 dB. This is compared to values of 15.48 dB and 14.75 dB for PA PAM-DMT with $R = 5$ and 10 iterations respectively.

The distributions of the PAPR values of PAM-DMT and PA PAM-DMT for an 8-PAM constellation order are shown

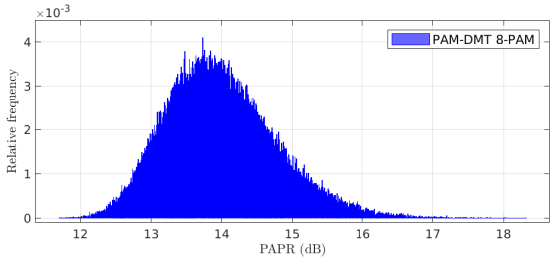

(a) PAM-DMT PAPR distribution without high peaks reduction.

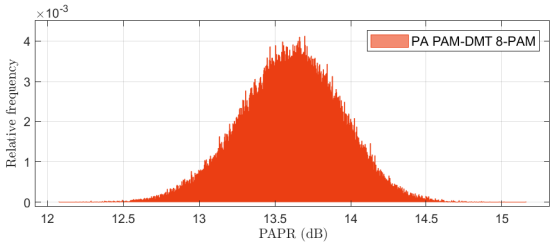

(b) PA PAM-DMT PAPR distribution with high peaks reduction.

Fig. 5. The distribution of the PAPR of optical PAM-DMT and PA PAM-DMT using 8-PAM, $U = 5$ data frames per block, N_{subs} = 127 active subcarriers, $L = 4$, IFFT length N_{IFFT} of 1024, $R = 10$ iterations and 10^5 frames.

in Fig. 5. The PAM-DMT PAPR range is between 11.69 and 18.32 in dB. However, with PAPR reduction scheme used in PA PAM-DMT, the PAPR spread is considerably reduced to values between 12.08 and 15.16 in dB. This is a reduction of more than 3 dB in the range of PAPR values which translates to reducing the peak power and the average transmitted optical power. This results in minimising the signal distortion caused by clipping of the front-end devices of the system hence improves the system performance.

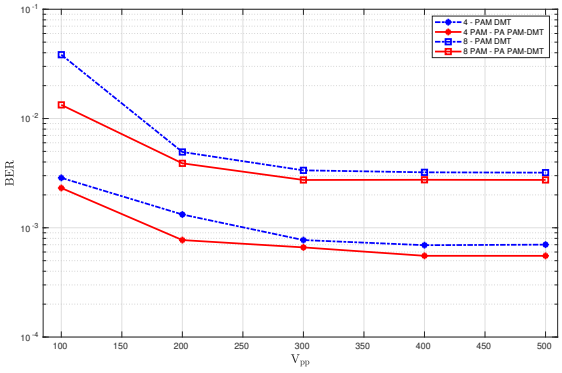

Fig. 6. Experimental BER plot for PAM-DMT and PA PAM-DMT using $[4, 8]$-PAM, $U = 5$ data frames per block, N_{subs} = 127 active subcarriers, $L = 4$ and IFFT length N_{IFFT} of 1024.

To determine the Bit Error Rate (BER) performance of PAM-DMT and PA PAM-DMT systems, the time domain signal $x[n]$ of both systems is normalised to unity prior to DAC. Then, the time domain signal is transmitted over a range of different transmit power levels (V_{pp}). The system SNR is calculated at different (V_{pp}) using the channel impulse response (CIR) at the corresponding (V_{pp}) as presented in

(6). This operation is carried out in the frequency domain at the receiver side after estimating the pilot sequence embedded to the transmitted signal using ML estimator to recover the data phase. The BER calculated from the equalized PAM demodulated symbols and plotted versus (V_{pp}).

The BER performance of the system shows that, the PA PAM-DMT BER is marginally better than that of the conventional PAM-DMT for $4-\mathrm{PAM}$ and $8-\mathrm{PAM}$ levels as shown in Fig. 6. The BER of both techniques saturates beyond input V_{pp} of 300 mV. The pilot assisted PA technique reduces the high PAPR peaks in PA PAM-DMT system as shown in Fig. 4 with system BER performance improvement as illustrated in Fig. 6. The system BER approaches an error floor due to the limited number of transmitted symbols and the nonlinearity effect of the light source.

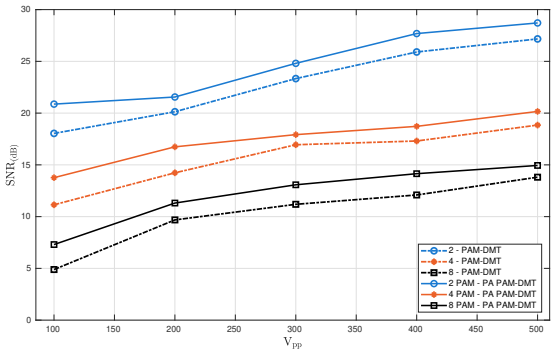

Fig. 7. Experimentally measured SNRs of PAM-DMT and PA PAM-DMT at a range of V_{pp} = [100 - 500] mV, sampling rate = 100 MHz and I_{DC} = 20 mA. PAPR reduction at $R = 10$ iterations, $U = 5$ data frames per block, upsampling factor $L = 4$, $N_{\mathrm{subs}} = 127$ active subcarriers and IFFT length N_{IFFT} = 1024.

The BER performance improvement in the PA PAM-DMT system is a result of reducing the high PAPR peaks which increases the peak-to-peak of the optical modulation amplitude of the signal and minimises the signal distortion from clipping hence, improving the SNR of the system. The SNR of the PA PAM-DMT is marginally higher than that of the basic PAM-DMT for all given input V_{pp} and modulation orders as shown in Fig. 7. This is evident by expressing the SNR in terms of PAPR as shown in (10). The system SNR as a function of the signal average power $P_{avg} = E[x^2(t)] = \sigma_x^2$ is:

$$SNR = \frac{|H_0|^2 \max[|x[n]|^2]}{\sigma_n^2 \times \mathrm{PAPR}} \tag{10}$$

where H_0 is the time invariant path-loss and σ_n^2 is the system noise variance which calculated using (9) [14]. PAPR reduction as seen in (10) results in an improvement in the system SNR. This expression is used to simulate the error performance presented in Fig. 8 using first order low pass filter and σ_n^2 = 1.1×10^{-5}. The simulation corroborates the experimental result of Fig. 6 that reduced PAPR does improve BER. However, the nonlinearity effect is not considered for

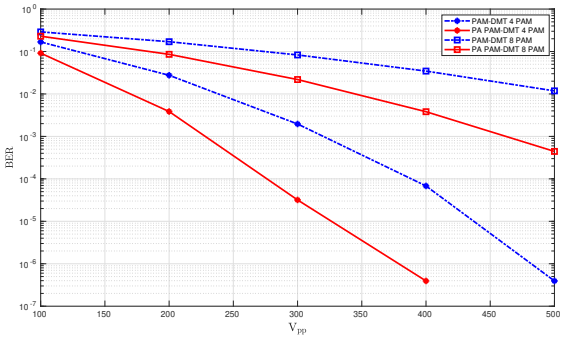

Fig. 8. BER simulation of PAM-DMT and PAPR reduced PA PAM-DMT measured at different values of V_{pp}, PAPR reduction at $R = 10$ iterations, upsampling factor $L = 4$, $N_{\mathrm{subs}} = 127$ active subcarriers and FFT length $N_{\mathrm{IFFT}} = 1024$.

the simulation. Hence, the BER in Fig. 8 does not approach an error floor as in Fig. 6.

Reducing the PAPR of the VLC system allows for higher input power levels for LEDs, increases the system SNR and minimises the non-linearity effects caused by the LED's upper and lower clipping points. In addition, the PAPR reduction has the potential to reduce the transmitted average optical power which results in increasing the reliability of the LED and hence, the life time of the LED.

VI. Conclusion

The high PAPR of the time domain signal of PAM-DMT $x[t]$ is studied and reduced using pilot assisted technique in PA PAM-DMT. The number of iterations R can be modified to obtain different levels of PAPR reduction i.e. a gain of 2.75 dB is achieved by $R = 10$ pilot iterations. This PAPR reduction is obtained with BER performance improvement. The SNR of the proposed scheme is higher than that of its counterpart. This is proven in an experimental proof-of-concept study for PA PAM-DMT system and compared with PAM-DMT system over a VLC channel.

Acknowledgment

The authors acknowledge the support by Jazan University, the faculty of Computer Science and Information Technology, Jazan, Kingdom of Saudi Arabia for funding this work.

References

[1] M. S. Islim, D. Tsonev, and H. Haas, "On the superposition modulation for ofdm-based optical wireless communication," in *2015 IEEE global conference on signal and information processing (GlobalSIP)*, pp. 1022–1026, IEEE, 2015.

[2] Z. Ghassemlooy, W. Popoola, and S. Rajbhandari, *Optical wireless communications: system and channel modelling with Matlab®*. CRC press, 2019.

[3] W. O. Popoola, Z. Ghassemlooy, and B. G. Stewart, "Pilot-Assisted PAPR Reduction Technique for Optical OFDM Communication Systems," *Journal of Lightwave Technology*, vol. 32, pp. 1374–1382, April 2014.

[4] S. C. J. Lee, S. Randel, F. Breyer, and A. M. J. Koonen, "Pam-dmt for intensity-modulated and direct-detection optical communication systems," *IEEE Photonics Technology Letters*, vol. 21, pp. 1749–1751, Dec 2009.

[5] J. Armstrong and B. J. Schmidt, "Comparison of asymmetrically clipped optical ofdm and dc-biased optical ofdm in awgn," *IEEE Communications Letters*, vol. 12, no. 5, pp. 343–345, 2008.

[6] S. K. Wilson and J. Armstrong, "Digital modulation techniques for optical asymmetrically-clipped ofdm," in *2008 IEEE Wireless Communications and Networking Conference*, pp. 538–542, 2008.

[7] X. Deng, S. Mardanikorani, G. Zhou, and J. M. G. Linnartz, "Dc-bias for optical ofdm in visible light communications," *IEEE Access*, vol. 7, pp. 98319–98330, 2019.

[8] J. Armstrong, "OFDM for optical communications," *Journal of Lightwave Technology*, vol. 27, pp. 189–204, Feb 2009.

[9] S. Dimitrov, S. Sinanovic, and H. Haas, "Clipping noise in ofdm-based optical wireless communication systems," *IEEE Transactions on Communications*, vol. 60, pp. 1072–1081, April 2012.

[10] N. R. Raajan, S. Prabha, and D. Meenakshi, "Improved performance in OFDM systems by PAPR reduction techniques," in *2013 International Conference on Computer Communication and Informatics*, pp. 1–4, Jan 2013.

[11] T. Zhang, Y. Zou, J. Sun, and S. Qiao, "Design of pam-dmt-based hybrid optical ofdm for visible light communications," *IEEE Wireless Communications Letters*, vol. 8, no. 1, pp. 265–268, 2018.

[12] W. O. Popoola, Z. Ghassemlooy, and B. G. Stewart, "Optimising ofdm based visible light communication for high throughput and reduced papr," in *2015 IEEE International Conference on Communication Workshop (ICCW)*, pp. 1322–1326, IEEE, 2015.

[13] Seung Hee Han and Jae Hong Lee, "An overview of peak-to-average power ratio reduction techniques for multicarrier transmission," *IEEE Wireless Communications*, vol. 12, pp. 56–65, April 2005.

[14] D. Tsonev, S. Videv, and H. Haas, "Unlocking spectral efficiency in intensity modulation and direct detection systems," *IEEE Journal on Selected Areas in Communications*, vol. 33, no. 9, pp. 1758–1770, 2015.